

Simplified Chirp Characterization in Single-shot Supercontinuum Spectral Interferometry

DinhDuy Tran Vu¹, Dogeun Jang¹, and Ki-Yong Kim^{1*}

¹ *Institute for Research in Electronics and Applied Physics,
University of Maryland, College Park, MD, 20742*

Single-shot supercontinuum spectral interferometry (SSSI) is an optical technique that can measure ultrafast transients in the complex index of refraction. This method uses chirped supercontinuum reference/probe pulses that need to be pre-characterized prior to use. Conventionally, the spectral phase (or chirp) of those pulses can be determined from a series of phase or spectral measurements taken at various time delays with respect to a pump-induced modulation. Here we propose a novel method to simplify this process and characterize reference/probe pulses up to the third order dispersion from a minimum of 2 snapshots taken at different pump-probe delays. Alternatively, without any pre-characterization, our method can retrieve both unperturbed and perturbed reference/probe phases, including the pump-induced modulation, from 2 time-delayed snapshots. From numerical simulations, we show that our retrieval algorithm is robust and can achieve high accuracy even with 2 snapshots. Without any apparatus modification, our method can be easily applied to any experiment that uses SSSI.

I. INTRODUCTION

Single-shot spectral interferometry (SSI) is an ultrafast optical method that can measure ultra-rapid refractive index transients induced by ultrashort laser pulses [1, 2]. This measurement can provide a direct view of how a laser-induced perturbation evolves in time and space in a single-shot. In this technique, a pump pulse induces a refractive index transient in a medium, and a chirped reference and a time-delayed replica (probe) pulse, upon which the pump-pulse-induced phase shift has been imposed, interfere in an imaging spectrometer, producing a spectral interferogram. The corresponding spatiotemporal (time and 1-dimensional space) evolution of refractive index transient is then reconstructed with frequency-to-time mapping or full Fourier transform methods [2]. In particular, supercontinuum (SC) light has been used for the reference and probe pulses to provide a temporal resolution better than ~ 10 fs [2]. This single-shot supercontinuum spectral interferometry (SSSI) and SSI techniques have been successfully applied to capture laser-induced double step ionization of helium [3], laser-heated cluster explosion dynamics [4], laser wakefields [5], optical nonlinearity near the ionization threshold [6], and electronic and inertial nonlinear responses in molecular gases [7–10]. SSI has been also used to capture terahertz waveforms in snapshots without pump-probe scanning [11, 12].

Unlike self-referencing nonlinear diagnostics such as FROG [13, 14] and SPIDER [15, 16], linear spectral interferometry including SSSI requires pre-characterized reference/probe pulses prior to its use. One method to pre-characterize a chirped probe in SSSI is to scan the delay between the pump-probe pulses while tracking a characteristic central extremum in the modulated

probe phase or spectrum [2]. This method can determine the spectral phase of SC probe light to arbitrary order [17]. However it relies on stationary-phase and small-perturbation approximations, which can be problematic when the phase modulation is too large or too asymmetric. In addition, this requires repetitive measurements over the entire chirp window for an accurate extraction of higher order dispersion coefficients. In particular, for a SC probe that has an extremely large bandwidth, a large number of pump-probe scans are necessary. This scanning method is impractical for use with low-repetition-rate laser sources.

For these reasons, we aim to develop a method that can simplify or avoid the pre-characterization process if possible and potentially to characterize both SC reference/probe pulses and pump-induced transients with a minimal number of repetitions.

II. BACKGROUND THEORY

In SSSI, the probe SC pulse, $E(t)$, is perturbed by a pump-induced modulation, $\Delta\Phi(t - \tau)$, applied at a time delay τ with respect to the probe pulse (see Fig. 1). The reference SC pulse, $E_r(t)$, precedes the pump in time and thus remains unaffected.

The perturbed probe pulse $\bar{E}(t)$ can be written as

$$\bar{E}(t) = E(t)e^{i\Delta\Phi(t-\tau)}, \quad (1)$$

where $E(t)$ is the unperturbed probe pulse. Then $\Delta\Phi(t)$, the same pump-induced modulation but applied at $\tau = 0$, can be extracted from the interference between the reference and probe pulses in the frequency domain as

$$\Delta\Phi(t) = -i \ln \left[\frac{F \{ |\bar{E}(\omega)| e^{i(\Delta\varphi_\tau(\omega) + \varphi(\omega))} e^{-i\omega\tau} \}}{F \{ |E(\omega)| e^{i\varphi(\omega)} e^{-i\omega\tau} \}} \right], \quad (2)$$

where F denotes the Fourier transform, $|\bar{E}(\omega)|$ and $|E(\omega)|$ is the spectral amplitude of the perturbed and un-

* kykim@umd.edu

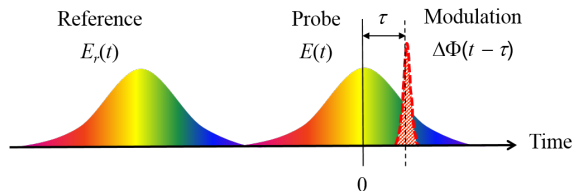


FIG. 1. Schematic of SSSI consisting of a chirped supercontinuum (SC) pulse (reference, $E_r(t)$) and a time-delayed replica pulse (probe, $E(t)$) upon which a pump-induced ultrafast modulation $\Delta\Phi(t - \tau)$ has been imparted at a time delay τ with respect to the probe.

perturbed probe pulses, respectively, that can be directly measured by a spectrometer; $\Delta\varphi_\tau(\omega)$ is the phase difference between the modulated probe and reference pulses at a given τ that can be obtained from an interferometer; and $\varphi(\omega)$ is the spectral phase of the unperturbed probe (or reference) pulse. Here to retrieve $\Delta\Phi(t)$, the spectral phase $\varphi(\omega)$ needs to be characterized. In general, the spectral phase of a chirped pulse can be expressed in a Taylor expansion around the central frequency ω_c as

$$\begin{aligned} \varphi(\omega) = & \varphi_0 + b_1(\omega - \omega_c) \\ & + b_2(\omega - \omega_c)^2 + b_3(\omega - \omega_c)^3 + \dots, \end{aligned} \quad (3)$$

where φ_0 is the absolute spectral phase; b_1 is the first order dispersion coefficient related to a pulse shift in time; b_2 and b_3 are the second and third order dispersion coefficients, respectively. Here the first two terms are not required in retrieving $\Delta\Phi(t)$, but b_2 and b_3 need to be characterized for SSSI operation.

In Eq. (2), it is important to note that the modulation $\Delta\Phi(t)$ remains unchanged even if the time delay τ changes. This is because the term $e^{-i\omega\tau}$ shifts the modulation occurring at $t - \tau$ back to t . In other words, $\Delta\Phi(t)$ must be uniquely retrieved from many different τ delayed shots if the spectral phase φ is correctly characterized.

For illustration, we consider a Gaussian-type phase modulation given by

$$\Delta\Phi(t - \tau) = A e^{-(t-\tau)^2/(2\sigma^2)}, \quad (4)$$

where we choose $A = 0.4$ and $\sigma = 50$ fs. Here the probe pulse is also a Gaussian pulse centered at 800 nm with a full-width-at-half-maximum (FWHM) bandwidth of 170 nm and chirped with $b_2 = 1000$ fs² and $b_3 = 400$ fs³. Figure 2(a) shows a series of differential probe power spectrum [17], $\Delta I(\omega)$, as a function of the pump-probe delay τ . Figure 2(b) shows two spectral line-outs at $\tau = 0$ fs and 400 fs. One prominent feature is that the position of the central minimum ω_0 shifts with respect to the pump-probe delay τ . Here the central minimum is defined as the point where $\Delta I(\omega)$ oscillates slowest; mathematically, it is given by the condition

$$\varphi'(\omega_0) = 2b_2(\omega_0 - \omega_c) + 3b_3(\omega_0 - \omega_c)^2 = \tau. \quad (5)$$

Therefore, by tracing ω_0 at each τ , one can determine b_2 and b_3 with a polynomial fit [17]. This method, however, is limited by the validity of the stationary phase approximation. Moreover, it is inefficient as only the central minimum/maximum point or at most some adjacent extrema are used in each shot for characterization.

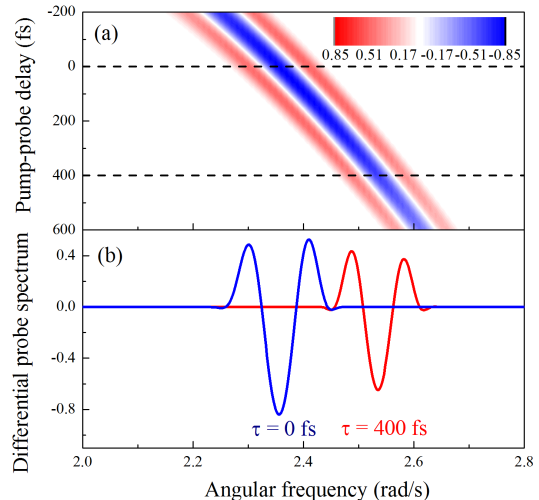


FIG. 2. (a) Simulated differential probe power spectrum, $\Delta I(\omega, \tau)$, modulated by a phase transient given by Eq. (4) as a function of pump-probe delay. The probe is chirped with $b_2 = 1000$ fs² and $b_3 = 400$ fs³. (b) Differential probe spectral line-outs at $\tau = 0$ fs and $\tau = 400$ fs

It is obvious that one needs the correct values of the second and third dispersion coefficients to properly characterize the phase modulation, but what is the consequence if the known values differ by Δb_2 and Δb_3 from the true ones? Our simulation shows that nonzero Δb_2 or Δb_3 lead to ambiguity in the retrieved modulation $\Delta\Phi(t)$. For illustration, we show the retrieved $\Delta\Phi(t)$'s from two different time delays $\tau = 0$ fs and $\tau = 400$ fs with $\Delta b_2 = 0$ fs², $\Delta b_3 = -40$ fs³ in Fig. 3(a) and $\Delta b_2 = -60$ fs², $\Delta b_3 = 40$ fs³ in Fig. 3(b). Those two retrieved $\Delta\Phi(t)$'s are different, and furthermore neither is identical to the true modulation. For a wider range of Δb_2 and Δb_3 , we quantify the difference in shape of the retrieved modulations obtained from multiple time-delayed shots by

$$\Delta S^2 = \int_{-\infty}^{\infty} \sum_{\tau} [\Delta\Phi_{\tau}(t) - \overline{\Delta\Phi}(t)]^2 dt, \quad (6)$$

where $\overline{\Delta\Phi}(t)$ is the average of $\Delta\Phi_{\tau}$ retrieved from all different time delays τ . This ΔS^2 strongly depends on how well the probe phase is characterized. For example, the dependence of ΔS^2 on both Δb_2 and Δb_3 is computed and shown in Fig. 3(c). It clearly shows a deep global minimum located at (0,0), which corresponds to the initially assigned probe phase ($b_2 = 1000$ fs² and

$b_3 = 400 \text{ fs}^3$). This shows that the modulations obtained from all different time delays converge only when the pulse's phase used for retrieval matches the true form. At the same time, the converged function represents the real form of modulation. A mathematical proof of this observation is provided in Appendix.

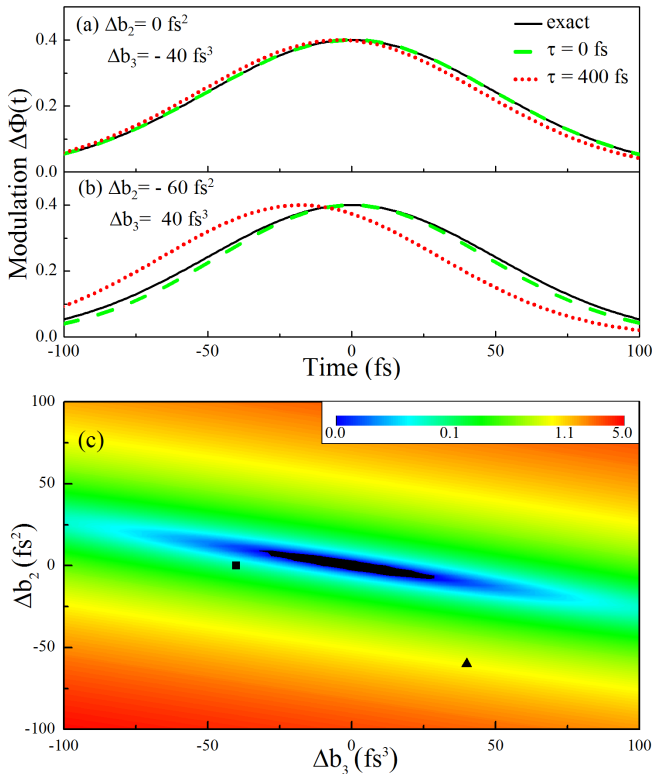


FIG. 3. (a), (b) Extracted modulations $\Delta\Phi(t)$ obtained from two different time-delayed shots at $\tau = 0 \text{ fs}$ (green dashed line) and $\tau = 400 \text{ fs}$ (red dotted line) using intentionally incorrect spectral phase coefficients, along with the correct modulation (black line). The modulations $\Delta\Phi(t)$ obtained from two shots of different time delay are nonidentical when Δb_2 or Δb_3 is non-zero. (c) The dependence of ΔS^2 on Δb_2 and Δb_3 shows a deep global minimum located at $(0, 0)$. The square and the triangle correspond to $(\Delta b_2, \Delta b_3) = (0, -40)$ and $(-60, 40)$ as illustrated in (a), (b) respectively.

III. ALGORITHM DETAILS

Experimentally, it is possible that modulations from different shots are similar in shape but slightly different in magnitude due to pump pulse power fluctuation. Therefore, the modulation extracted from each shot is normalized prior to comparison. We also emphasize that the retrieved modulation often exhibits smooth variations in the vicinity of the central extremum, but it is very noisy in the far away region. Therefore, in practice, only a region of interest is used for an input. This should cover as much meaningful features of modulation as possible but

be narrow enough to avoid too much noise.

One feature needs to be discussed is how to choose different time delays τ to optimize the operation of our algorithm. In a stationary phase approximation, the perturbed probe pulse can be expressed as [17]

$$\bar{E}(\omega) = E(\omega) - C \frac{\Delta\Phi(\omega - \omega_0)}{\sqrt{b_2'}} |E(\omega)| \times \exp \left[ib_2'(\omega - \omega_0)^2 + ib_3(\omega - \omega_0)^3 \right], \quad (7)$$

where C is a constant, $\Delta\Phi(\omega)$ is the Fourier transform of $\Delta\Phi(t)$ in the frequency domain, $b_2' = b_2 + 3b_3(\omega_0 - \omega_c)$, and ω_0 is given by $\varphi'(\omega_0) = \tau$. In the case of a small τ , ω_0 becomes close to ω_c and $b_2' \approx b_2$, and the dominant part containing the third-order dispersion $3b_3(\omega_c - \omega_0)(\omega - \omega_0)^2$ becomes insignificant. In that case, the third order dispersion is hard to be determined. Therefore, for an effective operation, we want the change caused by the third-order dispersion to be greater than its measurement error ε

$$\frac{3b_3(\omega_0 - \omega_c)}{b_2} > \varepsilon, \quad (8)$$

where $\omega_0 - \omega_c \approx \tau/(2b_2)$. Therefore, the time delay separation between two shots should be

$$\Delta\tau > \frac{\varepsilon b_2^2}{6b_3}. \quad (9)$$

Equation (9) establishes the relation between the time delay and experimental conditions. Furthermore, the upper limit of the time delay is fundamentally set by the probe pulse duration.

As illustrated in Fig. 3, the probe spectral phase can be found by minimizing ΔS^2 . This process can be performed by a genetic algorithm (GA). Figure 4 shows a diagram of our algorithm routine to characterize both probe and modulation simultaneously. First, the spectral modulations of probe $(\Delta\varphi_{s1}, \Delta\varphi_{s2}, \dots, \Delta\varphi_{sN})$ are measured at multiple pump-probe time delays τ_i . Along with an initial population of b_2 's and b_3 's, the corresponding temporal modulation functions $(\Delta\Phi_1, \Delta\Phi_2, \dots, \Delta\Phi_N)$ are constructed within Eq. (2). Then the GA is used to minimize ΔS^2 defined by Eq. (6). Finally, those b_2, b_3 that provides the global minimum of ΔS^2 will be selected for the best fitting parameters. Simultaneously, the $\bar{\Delta\Phi}(t)$ calculated from these optimized values is deemed to be the correct form of the applied modulation.

IV. PERFORMANCE TEST

In this section, we test the reliability of our algorithm with numerical simulations. Here we simulate two types of modulations. The first one mimics a Kerr-induced refractive index modulation, where the modulation is proportional to the intensity of a co-propagating pump

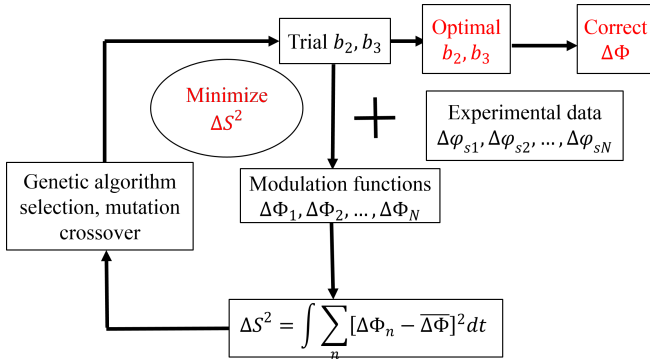


FIG. 4. Algorithm routine for simultaneous characterization of both probe chirp (b_2 and b_3) and modulation ($\Delta\Phi(t)$). It uses a genetic algorithm (GA) to minimize ΔS^2 such that the modulation functions obtained from all pump-probe delays can converge to equality.

pulse. The second one simulates a femtosecond photoionization process, where the modulation asymptotically approaches zero at $t \rightarrow -\infty$ and a non-zero value at $t \rightarrow \infty$. In both cases, the probe pulse is set to be the same as in the previous sections with $b_2 = 1000 \text{ fs}^2$ and $b_3 = 400 \text{ fs}^3$.

IV.1. Kerr-like Modulation

An intense laser pulse can induce a transient in the index of refraction of a medium it propagates through, leading to a phase modulation on the co-propagating probe pulse. We assume the modulation has a form of

$$\Delta\Phi(t) = A_1 e^{-at^4} [1 - b(t - t_0)] + iA_2 e^{-ct^2}, \quad (10)$$

with $A_1 = 0.2$, $a = 1.6 \times 10^{-7} \text{ fs}^{-4}$, $b = 5 \times 10^{-2} \text{ fs}^{-1}$, $t_0 = 30 \text{ fs}$, $A_2 = 0.1$, and $c = 2.5 \times 10^{-3} \text{ fs}^{-2}$. The imaginary part (second term) represents nonzero absorption in the medium. Here we assume the modulation is not symmetric in time. We also introduce a random error of $\leq 5\%$ to the simulated spectrogram to test the stability of our algorithm and a fluctuation of $\leq 10\%$ to the magnitude of $\Delta\Phi$ for each time-delayed shot.

We first test the convergence speed of our GA. In this simulation, each generation comprises 80 sets of b_2, b_3 with the search range of $600 - 1200 \text{ fs}^2$ for b_2 and $200 - 800 \text{ fs}^3$ for b_3 . We perform the simulation in three cases with different numbers of time-delayed shots, namely two shots at $\tau = 0$ and 400 fs , three shots at $\tau = 0, 400$ and 600 fs , and four shots at $\tau = 0, 400, 600$ and -200 fs . In each case, we use the same initial population that is intentionally chosen to be far away from the converged values. The optimized ΔS^2 at each generation is shown in Fig. 3a. Despite the unfavorable condition we set, ΔS^2 converges fast in all three cases after 15 generations.

In Figs. 5(b)-5(d), we show the optimized set of b_2^*, b_3^* , and the average modulation $\overline{\Delta\Phi}(t)$ obtained from two,

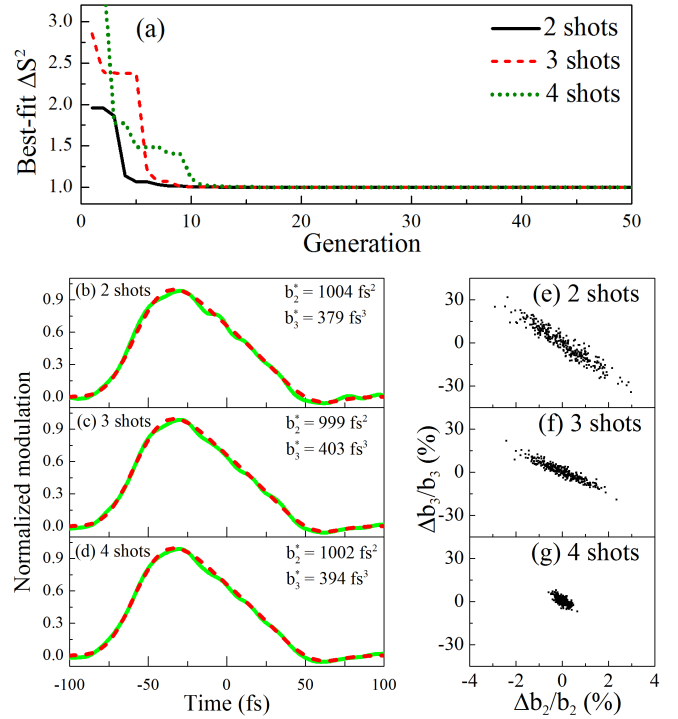


FIG. 5. (a) Minimal ΔS^2 after each generation when using data from two shots at $\tau = 0$ and 400 fs (black solid line), three shots at $\tau = 0, 400$ and 600 fs (red dashed line), and four shots at $\tau = 0, 400, 600$ and -200 fs (green dotted line). ΔS^2 is normalized to the final converged value. (b)-(d) The real part of reconstructed average modulation (green solid line) compared to the exact function (red dashed line) given by Eq. (10), with its best fitting parameters (b_2^* and b_3^*) obtained from 2, 3, and 4 shots, respectively, as defined in (a). (e)-(g) Distribution of retrieved (b_2, b_3) after 300 trials, corresponding to (b-d) respectively.

three, and four delayed shots. In this example, the second order dispersion coefficient b_2 can be characterized within a 1% error, and the shape of modulation can be reconstructed fairly well even with 2 shots. However, the third order dispersion coefficient b_3 , less significant compared to b_2 , suffers from a 5% error when only two shots are used only. It is noticeable that when 3 and 4 shots are used, the retrieval errors of b_2 and b_3 reduce to less than 1% and 2%, respectively.

We emphasize that the GA is so effective that it converges quickly to the almost exact global minimum of ΔS^2 regardless of the number of shots used. Note that we also introduce $\leq 10\%$ fluctuations to the modulation amplitude, but it is neutralized by the normalization step in our algorithm. Therefore, the retrieval error as shown previously is solely due to the random error introduced to the spectrogram. To examine how this error affects the retrieved values, we repeat the same simulation for 300 times and plot the extracted b_2 and b_3 in Figs. 5(e)-5(g). Firstly, compared to the typical uncertainty in b_2 (2%), b_3 spans much wider with the standard deviation

of $\sim 10\%$ in the case of 2 shots. This is understandable as the effect of third order dispersion on the spectra is quite small and can be overwhelmed by the random noise. Secondly, the overall certainty is diminished by increasing the number of snapshots. The error margins of retrieved b_2 and b_3 shrink significantly when the number of shots increase from 2 to 4, specially from $\sim 10\%$ to $\sim 2\%$ for b_3 . This is not surprising as the effect of random noise can be lessened by repetition. We note that our GA can always retrieve the exact b_2 and b_3 , and $\Delta\Phi(t)$ when no random fluctuation is included in the simulations.

IV.2. Femtosecond Stepwise Modulation

As a second example, we consider an ultrafast transient commonly observed in optical field ionization. In strong laser electric fields, atoms and molecules can be tunnel ionized, producing free electrons in continuum states. Macroscopically, the free electron density rises in time until the intense pulse passes by. The density modulation induced by the pump pulse can be picked up by a co-propagating probe pulse. For simplicity, we consider the following phase modulation caused by tunneling ionization,

$$|\Delta\Phi(t)| = \begin{cases} 0 & t \leq -20 \text{ fs} \\ 0.1(t+20) & -20 \text{ fs} < t \leq 20 \text{ fs} \\ 0.4 & t > 20 \text{ fs} \end{cases}. \quad (11)$$

Similar to the previous section, we simulate the spectrograms at different time delays and use data from 2, 3 or 4 shots to reconstruct the modulation. The spectrograms are also subject to $\leq 5\%$ random fluctuations. Our simulation results are presented in Figs. 6(a)-6(c). In the 2-shot case, the optimized b_2^* and b_3^* exhibit 1% and 10% errors, respectively. With the FWHM bandwidth of 170 nm, the fastest resolvable phase transient is ~ 5.5 fs for a Gaussian temporal modulation. For an abruptly changing function as in this example, its Fourier transform spreads much wider in the frequency domain than that of a Gaussian function (for instance $1/|\omega|$ for a step function in time). This leads to an even worse temporal resolution. Thus a relatively large uncertainty is expected in the extraction process. However, when using three or four shots, highly accurate characterization is possible.

In conclusion, our algorithm works well for two examples of ultrafast modulations even with $\leq 5\%$ random noise applied in the spectrograms. It will work equally well, we believe, for any reasonably shaped modulations. However, depending on the modulation shape, more than 2 shots are needed to obtain very high accuracy, especially when non-negligible random errors are present.

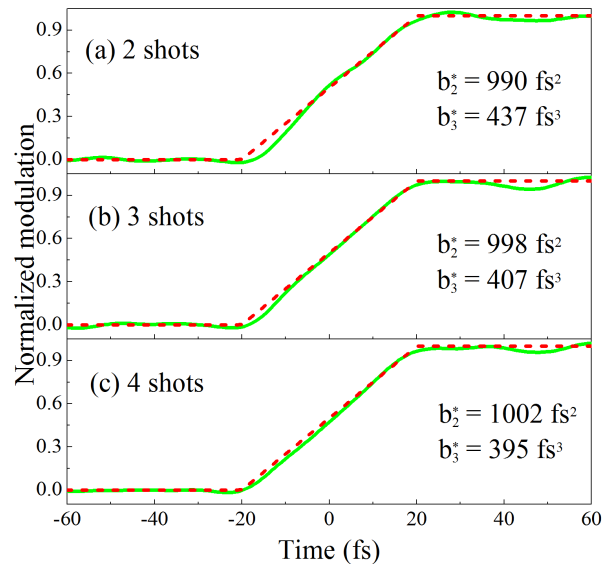


FIG. 6. Same as Figs. 5(b)-5(d) but the modulation function is given by Eq. (11).

IV.3. Extending the Number of Fitting parameters

In this section, we test the flexibility of the algorithm when more fitting parameters are introduced. In one possible scenario, the probe and reference pulses can be non-identical with different b_2 and/or b_3 . This disparity can occur when the reference and probe pulses pass through a beam splitter different numbers of times, thus leading to unequal dispersion. In that case, Eq. (2) needs to be modified as

$$\Delta\Phi(t) = -i \ln \left[\frac{F \{ |\bar{E}(\omega)| e^{i(\Delta\varphi_\tau + \varphi - \omega\tau)} \}}{F \{ |E(\omega)| e^{i(\varphi + \delta\varphi - \omega\tau)} \}} \right], \quad (12)$$

where $\delta\varphi$ is the phase difference between the probe and reference pulses. We estimate

$$\delta\varphi \approx B_2(\omega - \omega_c)^2, \quad (13)$$

where B_2 has an order of 10 fs^2 . In this example, there are three parameters to be optimized (b_2, b_3 and B_2). Here we choose $b_2 = 1000 \text{ fs}^2$, $b_3 = 400 \text{ fs}^3$, and $B_2 = 30 \text{ fs}^2$, with the same modulation and noise ($\leq 5\%$) as in Section IV.1 for simulation. The optimal parameters b_2, b_3 and B_2 retrieved from 2, 3 and 4 time-delayed shots are presented in Tab. I.

As shown in Tab. I, b_2 and B_2 can be determined within 2% regardless of the number of shots. Noticeably, when 3 or 4 shots are used, all three parameters can be obtained within 1% error. Note that b_2 is retrieved with a 3% difference, which is comparable to the 5% error obtained when the reference and probe pulses are set to be identical ($B_2 = 0$) in Section IV.1. Therefore, the addition of more chirp parameters does not significantly affect the performance of our algorithm.

TABLE I. Best-fit parameters (b_2^* , b_3^* , and B_2^*) retrieved with 2, 3, and 4 time-delayed shots when the probe and reference pulses are allowed to have second order dispersion coefficients different by B_2 .

	b_2^* (fs ²)	b_3^* (fs ³)	B_2^* (fs ²)
2 shots	1000	389	30.5
3 shots	997	398	29.8
4 shots	998	398	29.8

V. CONCLUSION

In summary, we have presented a simple method to determine both probe spectral phases and pump-induced modulations in a conventional SSSI setup. Our GA-based routine is shown to work for typical ultrafast modulations and capable of characterizing the probe phase with high accuracy. Also our algorithm can be easily modified to include more chirp parameters if necessary. With numerical simulations, we show that our algorithm is robust against random errors ($\leq 5\%$) and can provide satisfactory accuracy even with 2 time-delayed shots. With three or more shots, our algorithm can retrieve nearly the exact modulation and spectral phase. We believe our technique can be readily applied to any SSSI setup to simplify or eliminate its routine chirp characterization process.

APPENDIX: THE UNIQUENESS OF ΔS^2 MINIMUM

This section attempts to prove mathematically that the standard deviation ΔS^2 exhibits a zero value only when the phase function used in extraction has the correct form. Suppose that φ is slightly deviated as $\varphi \rightarrow \varphi + \delta\varphi$, then we have

$$\begin{aligned} |E(\omega)| e^{i(\varphi+\Delta\varphi)} e^{i\delta\varphi(\omega)} e^{-i\omega\tau} & \quad (14) \\ &= e^{i\delta\varphi(\omega)} e^{-i\omega\tau} F^{-1} \left[E(t) e^{i\Delta\Phi(t-\tau)} \right] \\ &= e^{i\delta\varphi(\omega)} \int M(\omega - \omega') e^{i\omega'\tau} |E(\omega')| e^{i\varphi(\omega')} d\omega', \end{aligned}$$

where $M(\omega) = F^{-1}[e^{i\Delta\Phi(t)}]$. The Fourier transform of

this term is given by

$$\begin{aligned} & F \left\{ E(\omega) e^{i(\varphi+\Delta\varphi)} e^{i\delta\varphi(\omega)} e^{-i\omega\tau} \right\} \quad (15) \\ & \propto \int F \left[\int M(\omega - \omega') E(\omega') e^{i[\varphi(\omega') - \omega'\tau]} d\omega' \right] C(t') e^{i\delta\tilde{\varphi}(t')} dt' \\ & \propto \int e^{i\Delta\Phi(t-t')} |E(t-t'-\tau)| e^{i\tilde{\varphi}(t-t'-\tau)} C(t') e^{i\delta\tilde{\varphi}(t')} dt', \end{aligned}$$

where $F \{ e^{i\delta\varphi(\omega)} \} = C(t) e^{i\delta\tilde{\varphi}(t)}$ and $E(t) = |E(t)| e^{i\tilde{\varphi}(t)}$. Generally, the modulation varies in a shorter time scale than the probe pulse, so $\tilde{\varphi}$ and $\delta\tilde{\varphi}$ vary much faster than $\Delta\Phi$. Using the stationary phase approximation, Eq. (15) can be approximated as

$$\begin{aligned} & F \left\{ E(\omega) e^{i(\varphi+\Delta\varphi)} e^{i\delta\varphi(\omega)} e^{-i\omega\tau} \right\} \quad (16) \\ & \propto e^{i\Delta\Phi(t-g)} \int |E(t-t'-\tau)| e^{i\tilde{\varphi}(t-t'-\tau)} C(t') e^{i\delta\tilde{\varphi}(t')} dt', \end{aligned}$$

where g is the point that contributes the most to the integral. Within the stationary phase approximation, this point can be given by

$$\delta\tilde{\varphi}'(g) - \tilde{\varphi}'(t-g-\tau) = 0. \quad (17)$$

As a result, Eq. (2) now gives

$$\begin{aligned} & \frac{F \{ E(\omega) \exp [i(\Delta\varphi + \varphi + \delta\varphi)] \exp(-i\omega\tau) \}}{F \{ E(\omega) \exp(i\varphi + i\delta\varphi) \exp(-i\omega\tau) \}} \quad (18) \\ & \approx \exp [i\Delta\Phi(t-g)]. \end{aligned}$$

Because g depends on τ according to Eq. (17), the extraction now produces different results at various time delays. Only when $\delta\varphi = 0$, making $C(t) e^{i\delta\tilde{\varphi}} \rightarrow \delta(t)$ and $g \rightarrow 0$, Eq. (18) yields the same function form regardless of τ .

FUNDING INFORMATION

National Science Foundation (NSF) (Award No. 1351455); Air Force Office of Scientific Research (AFOSR) (FA9550-16-1-0163).

-
- [1] J.-P. Geindre, P. Audebert, S. Rebibo, and J.-C. Gauthier, *Opt. Lett.* **26**, 1612 (2001).
 [2] K. Y. Kim, I. Alexeev, and H. M. Milchberg, *Appl. Phys. Lett.* **81**, 4124 (2002).
 [3] K. Y. Kim, I. Alexeev, and H. M. Milchberg, *Opt. Express* **10**, 1563 (2002).
 [4] K. Y. Kim, I. Alexeev, E. Parra, and H. M. Milchberg, *Phys. Rev. Lett.* **90**, 023401 (2003).
 [5] N. H. Matlis, S. Reed, S. S. Bulanov, V. Chvykov, G. Kalintchenko, T. Matsuoka, P. Rousseau,

- V. Yanovsky, A. Maksimchuk, S. Kalmykov, et al., *Nat. Phys.* **2**, 749 (2006).
 [6] J. K. Wahlstrand, Y.-H. Cheng, Y.-H. Chen, and H. M. Milchberg, *Phys. Rev. Lett.* **107**, 103901 (2011).
 [7] Y.-H. Chen, S. Varma, A. York, and H. M. Milchberg, *Opt. Express* **15**, 11341 (2007).
 [8] J. K. Wahlstrand, Y.-H. Cheng, and H. M. Milchberg, *Phys. Rev. A* **85**, 043820 (2012).
 [9] J. K. Wahlstrand, S. Zahedpour, Y.-H. Cheng, J. P. Palastro, and H. M. Milchberg, *Phys. Rev. A* **92**, 063828

- (2015).
- [10] S. Zahedpour, J. K. Wahlstrand, and H. M. Milchberg, *Opt. Lett.* **40**, 5794 (2015).
 - [11] N. H. Matlis, G. R. Plateau, J. van Tilborg, and W. P. Leemans, *J. Opt. Soc. Am. B* **28**, 23 (2011).
 - [12] S. Zheng, X. Pan, Y. Cai, Q. Lin, Y. Li, S. Xu, J. Li, and D. Fan, *Opt. Lett.* **42**, 4263 (2017).
 - [13] R. Trebino and D. J. Kane, *J. Opt. Soc. Am. A* **10**, 1101 (1993).
 - [14] T. C. Wong, M. Rhodes, and R. Trebino, *Optica* **1**, 119 (2014).
 - [15] C. Iaconis and I. A. Walmsley, *Opt. Lett.* **23**, 792 (1998).
 - [16] G. Stibenz and G. Steinmeyer, *Opt. Express* **12**, 6319 (2004).
 - [17] J. K. Wahlstrand, S. Zahedpour, and H. M. Milchberg, *J. Opt. Soc. Am. B* **33**, 1476 (2016).